RSC Advances

ROYAL SOCIETY OF CHEMISTRY

www.rsc.org/advances

Temperature-controlled giant thermal magnetoresistance behaviors in doped zigzag-edged silicene nanoribbons

X. F. Yang[1], X. Zhang [1], X. K. Hong [1], Y. S. Liu[1],*

J. F. Feng[1],† X. F. Wang[2],‡ and C. W. Zhang[3]

[1] *College of Physics and Engineering,*

Changshu Institute of Technology and Jiangsu Laboratory

of Advanced Functional materials, Changshu 215500, China

[2] *Department of physics, Soochow University, Suzhou 215006, China*

[3] *School of Physics and Technology,*

Univeristy of Jinan, Jinan, Shandong 250022, China.

Abstract

Based on the nonequilibrium Green's function (NEGF) method combined with the density functional theory (DFT), we investigate the spin-dependent thermoelectric transport properties of the zigzag-edged silicene nanoribbons (ZSiNRs) doped by a Al-P bonded pair at different edge positions. For the ferromagnetic (FM) configuration, the strong quantum destructive interference effects between the localized states induced by the Al-P bonded pair and side quantum states results in the appearance of the spin-dependent transmission dips near the Fermi level. This fact leads to the simultaneous enhancements of the spin-filter efficiency and spin Seebeck coefficient at the Fermi level, meanwhile their signs are dependent on the doping positions. Moreover, for the antiferromagnetic (AFM) configuration, the spin-dependent transmission peaks with the ordinary lorentzian shapes near the Fermi level can be introduced by the Al-P bonded pair. Interestingly, a pure spin current in the doped AFM ZSiNRs can be achieved by modulating the temperature. In this case, the spin-filter efficiency can reach infinite, meanwhile the thermal magnetoresistance (TMR) between the FM and AFM configurations can also reach infinite.

PACS numbers: 85.75.-d; 72.15.Jf; 85.80.-b

Keywords: Zigzag-edged silicene nanoribbons; Thermal magnetoresistance; Spin-filter efficiency; Spin Seebeck effects

I. INTRODUCTION

Since graphene, a monolayer of carbon atoms with the honeycomb lattice, is experimentally realized in 2004 [1], the graphene-like materials have been widely studied in recent years. Among them, silicene, the monolayer honeycomb structure of silicon, has been proposed as an important material due to its graphene-like features and the compatibility to silicon-based electronic devices [2]. In addition to similar properties such as high mobility charges, quantum spin Hall effect, and a Dirac core in band structures, silicene has a large spin-orbit gap at the Dirac point [3], experimentally accessible quantum spin Hall effect [4], electrically tunable band gap [5] and a valley-polarized metal phase [6]. Different from the planar structure of graphene, silicene has a low-buckled structure resulting from the weaker π-π overlaps than graphene. Until now, though the free-standing silicene has yet not been reported experimentally, the high-quality silicene sheets with the low-buckled structure have been successfully created on the silver [7], ZrB_2 [8], and Ir(111) substrates [9]. Earlier experiments have also demonstrated the capability of fabricating the one-dimensional silicene nanoribbons (SiNRs) [10, 11]. The SiNRs with different edges exhibit the entirely different electronic structures. For example, the armchair-edged SiNRs (ASiNRs) are metallic or semiconductors by modulating their width. However, for the zigzag-edged SiNRs (ZSiNRs), the antiferromagnetic (AFM) semiconducting state is the stable ground state. Using an external magnetic field, we can realize the switch between the ferromagnetic (FM) excited state and the AFM ground state.

In addition, the transport properties of SiNRs or graphene nanoribbons (GNRs) have also attracted much attention in recent years. For instance, the single-spin electric current in the doped zigzag-edged GNRs (ZGNRs) shows the negative differential resistance (NDR), while the other-spin electric current is monotonically increased with the bias voltage [12,

13]. The strong spin-dependent NDR is also reported in composite armchair GNRs-based superlattices with a set of ferromagnetic insulator strips [14]. Kang *et. al.* presented a first-principles calculation to investigate the symmetry-dependent transport properties of ZSiNRs [15]. Even-number and odd-number ZSiNRs show different current-voltage relationships, which are attributed to the different parity of the wave functions. The magnetoresistance in even-number ZSiNRs can reach $10^7\%$ [15]. By changing the edge spin direction of ZSiNRs, a giant magnetoresistance can be predicted [16]. Very recently, Chen *et. al.* also found a very large magnetoresistance in monohydrogenated ZSiNRs doped by the elements in groups III and V [17].

Ab initio molecular dynamics simulations show the hydrogen (H)-passivated SiNRs have the very good stability at the high temperature region, indicating the possibility of using SiNRs as potential thermoelectric materials [18]. Recent theoretical researches have shown that the thermoelectric effects of pristine ZSiNRs in the low-energy AFM state can be obviously enhanced due to the existence of the energy gap at the Fermi level [19]. For the pristine ZSiNRs in the FM state, the thermoelectric effects are very weak due to a conductance platform at the Fermi level. However, by the edge doping, the spin Seebeck effect (SSE) can be obviously enhanced [20]. Here, the SSE is defined by the generation of the spin voltage arising from a temperature difference, which was first observed experimentally in a metallic magnet by using a spin detection technique [21]. This innovative experiment immediately inspires abundant theoretical and further experimental investigations in various systems [22–31]. Recently, Zhao *et. al.* found a large thermal magnetoresistance (TMR) effect under a small local gate voltage when the ZGNR is transformed between the FM state and the AFM ground state [32].

Edge modifications, structure defects and systematic doping can effectively alter the electronic structures and magnetic properties of GNRs and SiNRs. In the asymmetrical-

ly hydrogenated ZGNR homojunction, an intrinsic spin-filter effect is exhibited [33]. In addition, the half-metallicity is also reported in the ZGNRs with divacancies and divacancies combined with the Stone-Wales-like (SW) defects at the Fermi level [34]. Among these methods, the chemical doping is the more frequently performed to change the electron structures and transport properties. For example, Zheng et. al. reported a systematic study of the ZGNRs with single and multiple dopants [35]. These dopants induce bound states and qusibound states, resulting in the dips and peaks in the transmission spectra. Experimentally, by using the atmospheric-pressure chemical vapor deposition, Lv et. al. described the synthesis of large-area, highly-crystalline monolayer N-doped graphene (NG) sheets, and the localized states in the conduction band induced by N doping could be revealed by the scanning tunneling microscopy and spectroscopy [36]. To keep the whole system isoelectric, Dutta et. al. performed a first-principles method to investigate the ZGNRs with the B-N chemical dopants, and found the doping concentrations and positions can regulate the electronic structures of ZGNRs [37]. The effects of these chemical dopants have also been investigated experimentally in nanotubes [38]. And likewise, the chemical doping is also way of improving electronic and transport properties of SiNRs. Very recently, Zberecki et. al. investigated the spin effects in thermoelectric properties of ZSiNRs with Al or P doping, and the results showed that the spin thermopower can be obviously enhanced by these impurities [39]. A quantum-mechanical Landauer-Büttiker approach has been performed to evaluate the conductivities of doped SiNRs with various impurity concentrations including B, N, Al, and P substitutions. The results showed that these substitutional doping could widen transport gaps of silicene [40].

In this paper, motivated by the advances of recent experimental realizations and widely theoretical works of ZSiNRs, we present a first-principles study of the spin-dependent thermoelectric transport properties of the ZSiNRs doped by the Al-P bonded pair at different

doping positions, keeping the while system isoelectric. For the FM configuration, we find that the spin-filter efficiency (SFE) and SSE at the Fermi level can be obviously enhanced by doping the Al-P bonded pair . These results are attributed to the appearance of the spin-dependent transmission dips originating from the strong destructive interference effects. In addition, the signs of SFE and SSE are dependent on the doping positions. More interestingly, a pure spin current without an accompanying charge current in the doped AFM ZSiNRs is achieved by modulating the temperature. In this case, the SFE can reach infinite. Meanwhile, the TMR between the FM and AFM configurations can also reach infinite.

II. MODEL AND COMPUTATIONAL METHODS

As illustrated in Figs. 1 (a) and (b), we divide the n-ZSiNR in FM and AFM states into three regions: left semi-infinite electrode, central scattering region, and right semi-infinite electrode. n in n-ZSiNR denotes the width of ZSiNRs, and here it is chosen to be 6 in our work. The Atomistix ToolKit (ATK) package based on the NEGF combined with the DFT is performed to obtain the spin-polarized transport properties [41, 42]. The electron wave function is expanded in a basis set of double zeta orbitals plus one polarization orbital (DZP). To separate ZSiNRs in neighbor suppercells and ensure the suppression of the coupling between them, a vacuum region of width 15 $\AA$ is adopted. The energy cutoff is chosen to be 150 Ry and the size of the mesh grid in k space for the electrode parts is $1 \times 1 \times 100$. All the two-probe structures doped by the chemical dopants are fully relaxed until the forces are smaller than 0.02 eV/Å on each atom. The spin-dependent transmission function τ_σ is calculated by [41]

$$\tau_\sigma(E) = \frac{e^2}{h} Tr[\mathbf{\Gamma}^L_\sigma(E)\boldsymbol{G}^r_\sigma(E)\mathbf{\Gamma}^R_\sigma(E)\boldsymbol{G}^a_\sigma(E)], \quad (1)$$

$\mathbf{\Gamma}_\sigma^{L(R)}(E)$ Green's function is obtained by $\boldsymbol{G}_\sigma^r(E) = [E\boldsymbol{I} - \boldsymbol{H} + i(\mathbf{\Gamma}_\sigma^L + \mathbf{\Gamma}_\sigma^R)/2]^{-1}$, where $\boldsymbol{I}$ is the unit matrix and $\boldsymbol{H}$ the Hamiltonian of the scattering region. The advanced Green's function $\boldsymbol{G}_\sigma^a(E)$ is obtained by $\boldsymbol{G}_\sigma^a = [\boldsymbol{G}_\sigma^r]^\dagger$. The spin-filter efficiency (SFE) at the Fermi level is given by,

$$SFE = \frac{\tau_\uparrow - \tau_\downarrow}{\tau_\uparrow + \tau_\downarrow}|_{E=E_F} \times 100\%. \tag{2}$$

When a thermal bias ΔT is applied across these two-probe devices, the spin-polarized current is,

$$I_\sigma = \frac{e}{h}\int dE(f_L - f_R)\tau_\sigma(E) \tag{3}$$

where $f_{L(R)}$ is the Fermi-Dirac distribution of the left (right) electrode. The SFE under a thermal bias ΔT is defined as,

$$\eta(T, \Delta T) = \frac{I_\uparrow(T, \Delta T) - I_\downarrow(T, \Delta T)}{I_\uparrow(T, \Delta T) + I_\downarrow(T, \Delta T)}. \tag{4}$$

Using an external magnetic field, we can force the AFM ground state to be a FM excited state. Thus the TMR at the different difference is defined as [43]

$$TMR(T, \Delta T) = \frac{|I_{FM}(T, \Delta T)| - |I_{AFM}(T, \Delta T)|}{|I_{AFM}(T, \Delta T)|} \tag{5}$$

where $I_{FM(AFM)}(= I_\uparrow + I_\downarrow)$ is the total electric current of the FM (AFM) configuration under a thermal bias ΔT. An experiment measurement for the magnetoresistance in graphene has been reported [44]. In addition, the spin-dependent Seebeck coefficient S_σ can be obtained by assuming a spin thermovoltage ΔV_σ induced by the thermal bias ΔT, letting $I_\sigma(\Delta V_\sigma, T)|_{\Delta T=0} + I_\sigma(\Delta T, T)|_{\Delta V_\sigma=0} = 0$. After expanding the Fermi-Dirac distribution function to the first order in ΔT and ΔV_σ, we have

$$S_\sigma = -\frac{1}{eT}\frac{L_{1\sigma}(\mu, T)}{L_{0\sigma}(\mu, T)}, \tag{6}$$

where $L_{\nu\sigma}(\mu, T) = -\int dE\{\partial f(E, \mu, T)/\partial E\}(\epsilon - \mu)^\nu \tau_\sigma(E)(\nu = 0, 1)$. μ is the chemical potential of the electrodes.

RESULTS AND DISCUSSIONS

As illustrated in Fig. 1 (c), the pristine ZSiNR and three different doping positions of the Al-P bonded pair in ZSiNRs are considered in this work. For the pristine ZSiNR, the optimized Si-Si bond length is about 2.28 $\mathring{A}$, and the buckled height is about 0.45$\mathring{A}$. These parameters are in consistent with the previous results [45]. After a Al-P bonded pair is doped, the optimized structures at the doping regions show that the band lengths are effectively amended. For example, the P-Si bond length is shorter than the intrinsic Si-Si bond, while the Al-Si bond length is longer than it. The Al-P bond length in the (1,2) position is smaller by 0.09 $\mathring{A}$ in comparison to that in the (2,3) and (3,4) doping positions. In addition, it is well known that the spin denisty is mainly accumulated in the edge Si atoms for the pristine FM ZSiNR, as depicted in Fig. 2(a1). The corresponding transmission spectrum shows a metallic behavior, and $\tau_\sigma(=1)$ at the Fermi level is the spin degenerate. Therefore, the SFE at the Fermi level at the low temperature regime is near zero. In addition, a wider transmission peak is located at about E= -0.2 eV and a narrower transmission peak at about E= 0.15 eV (see Fig. 2(a3)). At same energy positions, there exist two DOS peaks (see Fig. 2(a2)). We also plot S_σ as a function of energy at $T = 70K$ in Fig. 2(a4). A negative maximum of $S_\uparrow(S_\downarrow)$ is located in the below transmission peak in the negative (positive) energy region and a positive maximum of $S_\uparrow(S_\downarrow)$ in the above the transmission peak in the negative (positive) energy region. These numerical results can be well explained by,

$$S_\sigma(E) \simeq -\frac{\pi^2 k_B^2 T}{3e}\frac{\tau'_\sigma(E)}{\tau_\sigma(E)}. \quad (7)$$

The above equation clearly shows that S_σ is related not only to the magnitude of $\tau_\sigma(E)$ but also to its slope at energy E. For example, $S_\uparrow$ has a negative value due to $\tau'_\sigma(E) > 0$ in the below transmission peak at $E = -0.2eV$. When the Al-P bonded pair is doped at the

(1,2) and (2,3) positions, the spin polarization of the edge Si atom near the doping atom is obviously weaken (see Figs. 2(b1) and (c1)). The edge magnetism can be restored when the doping moves to the (3,4) position, as shown in Fig. 2(d1). In addition, it is interesting is that some localized quantum states appear and then induce some narrower DOS peaks (see Fig. 2(b2)). We also note that some spin-dependent Fano dips in the transmission spectra near these quantum states can be induced as shown in Fig. 3(b3)), which come from the quantum destructive interference effects between these localized quantum states and their neighboring the continuum state. Similar results are also reported in the mesoscopic systems [46]. For the (1,2) doping position, a spin-down transmission dip appears close to the Fermi level at $E = 0.03eV$, meanwhile $\tau_{\uparrow}$ is nearly invariable at this energy region. Thus, the SFE at the Fermi level reaches 67%. The corresponding local density of states (LDOSs) of spin-up and spin-down components at $E = 0.03eV$ are shown in Fig4. (a) and (b). We indeed find that a spin-down localized state is formed at the edge with the doping, and the LDOS is suppressed at the region near the right electrode. For the spin-up case, though the LDOS is obviously suppressed at the Al and P atoms, it is enhanced the sub-edge Si atoms. Meanwhile, compared with the pristine case, the slope of $\tau_{\downarrow}$ at the Fermi level is obviously enhanced, and is negative. According to Eq. (7), $S_{\downarrow}$ is positive, and can be enhanced to 78.7 $\mu V/K$ at $T = 70K$, while $S_{\uparrow}$ has a small value about $-1.7\mu V/K$. When the Al-P bonded pair is doped at the position (2,3), a spin-up transmission dip is located at $E = -0.04eV$, and the spin-down transmission nearly remains unchanged. At the Fermi level, the SFE becomes negative and about -63%. In Figs. 3 (c) and (d), we show the spin-up and spin-down LDOSs at $E = -0.036eV$ for the (2,3) doping position. For the spin-up case, a localized state is formed, and its LDOS is suppressed near the doping position. The spin-down LDOS nearly remains unchanged along the bottom Si atoms, resulting in a larger electron transmission probabilities for the spin-down electrons at $E = -0.036eV$.

In addition, since the slope of $\tau_\downarrow$ at the Fermi level is positive, $S_\uparrow$ has a negative value $-46.8\mu V/K$. Meanwhile, $S_\downarrow$ has a small value. This fact results in $|S_S| \simeq |S_C|$ at the Fermi level. Here $S_{S(C)}(=(S_\uparrow - (+)S_\downarrow)/2)$ is the spin (charge) Seebeck coefficient [47]. Therefore the signs of the SFE and SEE can be modulated by changing the doping positions of the Al-P bonded pair. When the doping position moves to (3,4), the transmission dips are far away from the Fermi level (see Fig. 2(d3)), leading to the weaker the SFE and spin-dependent Seebeck effects at the Fermi level. To further conform the existence of the localized state, as an example, we plot the spin-resolved band structures of the central scattering region with the doping at (1,2) as an unit cell. A spin-down flat band appears near and above the Fermi level, indicating a localized state is formed. The wave function of the spin-down band is plotted in Fig. 4(d). We find that the wave functions of spin-down electrons only occupy the several atoms near the doping atoms, and they are obviously suppressed on the edge region of the central scattering region. By way of contrast, for the spin-up component, the localized state can not be formed. We clearly see that the wave function of spin-up electrons are enhanced near the edge of the central region, though the wave function of the spin-up electrons are obviously suppressed (see Fig. 4 (c)).

For the AFM configuration, the spin with different direction is distributed on the edge Si atoms (see Fig. 5), and the Al-P bonded pair in the (1,2) and (2,3) doping positions can induce the suppression of the spin density near the doping atoms, as illustrated in Figs. 3 (b1) and (c1). Similar to the FM case, the spin on edge Si atoms can also be restored when the doping position moves to (3,4). It well known that the spin is degenerate for the pristine ZSiNR, and an obvious transmission and DOS gaps with the width of 0.26 eV is opened. The DOS spectrum shows a similar behavior as the transmission spectrum. In Fig. 5 (a4), we plot the S_σ as a function of energy E. Due to a rapid changing of τ_σ near the edge of the transmission gap, $|S_\sigma|$ is enhanced to about 1500 $\mu V/K$ near the Fermi level

and even $|S_\sigma|$ at the Fermi level can also reach 228 $\mu V/K$. When the Al-P bonded pair is doped at the position (1,2), the spin-dependent DOS spectrum shows that the some new quantum states appear not only in the outside of the gap but also in the inside of the gap (see Fig. 5(b2)). The quantum destructive interference effect between these quantum states in the outside of the gap and their neighboring quantum states lead to the transmission dips at these special energy positions. However, the quantum states in the gap induce some transmission peaks due to the absence of their neighboring quantum states (see Fig. 5(c2)). We also note that there is a spin-up (spin-down) transmission peak below (above) the Fermi level. It can induce an obvious enhancement of the spin Seebeck effect at the Fermi level, which is ascribed to the inverse sign of $S_\uparrow$ and $S_\downarrow$ due to $\tau'_\uparrow(E_F) < 0$ and $\tau'_\downarrow(E_F) > 0$. Therefore, in this case, the spin Seebeck coefficient is larger than the corresponding charge Seebeck coefficient. For example, at T=70K, $|S_S|$ is about 397 $\mu V/K$, while $|S_C|$ is about 176 $\mu V/K$ (see Fig. 5(d2)). When the Al-P bonded pair is doped at the position (2,3), it is interesting that the spin-up transmission peak appears above the Fermi level, while the spin-down conductance transmission peak appears below and a little bit far away from the Fermi level. Thus, the spin-down Seebeck coefficient at the Fermi level is strongly enhanced to 964 $\mu V/K$ at $T = 70K$. Even if the spin-dependent conductance transmission peaks are far away from the Fermi level for the doping position (3,4), S_σ at the Fermi level is still enhanced. In order to further evidence the importance of our findings, as an example, we plot the spin-dependent transmission function as a function of the electron energy for the single P and Al doping at position 1 and 2 in Figs. 6(a) and (c). After optimization, the P-Si bond lengths are nearly equal to the intrinsic Si-Si band lengths, while Al-Si bond lengths are obviously increased (see Figs. 6(b) and (d)). Importantly, we find that only spin-up transmission peaks (for the Al doping) and only spin-down transmission peaks (for the P doping) can be induced. These results indicate that the spin Seebeck effects are not larger

than the corresponding the charge Seebeck effects in these single atom dopants.

Though $|S_\sigma|$ of AFM ZSiNRs at the Fermi level is larger than that of FM ZSiNRs, we note that this fact is due to the exceptionally low transmission at the Fermi level. In the following, we will mainly focus on the thermally driven current in the FM and AFM ZSiNRs with Al-P bonded pair doping. When a thermal bias is provided between the two electrodes, the spin-dependent electric current can be obtained by Eq. (3). In the low-temperature linear region, I_σ is simplified as [48]

$$I_\sigma \simeq \frac{\Delta T}{2\pi k_B T}[\frac{\pi^2}{3}(k_B T)^2 \tau_\sigma^{'}(E_F)], \tag{8}$$

Different from Eq. (7) for the expression of S_σ, the thermal-bias-induced current I_σ is only related to that the slope of τ_σ at the Fermi level. The direction of the current is dependent on the sign of $\tau_\sigma^{'}$ at the Fermi level. $I_\sigma > 0$ means that electrons with the spin index σ flow from the left (high-temperature) to the right (low-temperature) electrodes, meaning a n-type thermoelectric devices for the spin index σ. When I_σ is negative, indicating that the electrons with the spin index σ flow from the right (low-temperature) to the left (high-temperature) electrodes. Actually, one can also think that the holes with the spin index σ flow from the left (high-temperature) to right (low-temperature) electrodes. A p-type thermoelectric device for the spin index σ is achieved. In Fig. 7, we plot I_σ of the doped FM (left column) and AFM (right column) as functions of ΔT for $T = 70K$. Here we do not present the results of the pristine ZSiNR due to $\tau'(E_F) \simeq 0$. For the FM configuration, I_σ has a perfectly linear relation to ΔT, and the results can be well explained by Eq. (8). When the Al-P bonded pair is doped at the position (1,2), $I_\uparrow$ is near zero due to $\tau_\uparrow^{'} \simeq 0$, but $I_\downarrow$ has a negative value because of $\tau_\downarrow^{'} < 0$. The SFE under the thermal bias [0,25] K is almost kept at a constant about -1.24 (see the red solid line in Fig. 8(a)). For the (2,3) and (3,4) doping positions, the absolute values of SFE in the thermal bias region is lesser

than 1 due to the same flowing direction of the current with the different spins. The linear relations between I_σ and ΔT for the AFM configuration are broken, and I_σ is very small (see the right column of Fig. (7)). More interestingly, when the (1,2) position is doped by the Al-P bonded pair, the charge current is zero at $\Delta T = 20.6K$. In this case, the spin-up electrons and spin-down electrons with same probabilities flow along the opposite directions. Therefore, according to Eqs. (4) and (5), the SFE can reach infinite (see Fig. 8(c)), and TMR between the FM and AFM states can also reach infinite due to $I_{AFM} = I_\uparrow + I_\downarrow = 0$ (see Fig. 8(b)). In Fig. 8(d), we plot TMRs of the three doped ZSiNRs as functions of T for the fixed ΔT. It is found that TMR is monotonically increased for position (1,2) and (3,4) as T is reduced. While for the position (2,3), the maximum of TMR emerges at T= 75K. For the position (1,2), the TMR is rapidly enhanced at about 70K. This result is due to the appearance of the nearly pure spin current. These results manifest that SFE and TMR can be effectively enhanced in the Al-P doped ZSiNRs by tuning the temperature. Especially it is interesting that the SFE in the doped AFM ZSiNRs can even reach infinite at a certain temperature, and then the corresponding TMR between the FM and AFM states can also reach infinite.

In conclusion, based on the nonequilibrium Green's functions (NEGF) combined with the density-functional theory (DFT), we investigate the SSE and thermal-bias-induced spin transport properties of the FM and AFM SiNRs doped by a Al-P bonded pair in different edge regions. It is found that the SFE and SEE are obviously enhanced, and their signs are related to the doping positions. More interestingly, the SFE in the doped AFM SiNRs can reach infinite by modulating the temperature. This behavior is due to the appearance of the pure spin current without an accompanying charge current. As a result, the TMR between FM and AFM states can also reach infinite.

ACKNOWLEDGMENTS

The authors thank the support of the National Natural Science Foundation of China (NSFC) under Grants Nos. 61404012, 11347021, 11247028, 61306122, and 91121021. Y. S. Liu also acknowledge the support of the Jiangsu Qing Lan and Jiangsu Province Technology Hall Projects.

* Electronic address: ysliu@cslg.edu.cn

† Electronic address: fengjinfu@cslg.edu.cn

‡ Electronic address: xf_wang1969@yahoo.com

[1] K. S. Novoselov, A. K. Geim, S. V. Morozov, D. Jiang, Y. Zhang, S. V. Dubonos, I. V. Grigorieva, and A. A. Firsov, Science 306, 666 (2004).

[2] M. Topsakal and S. Ciraci, Phys. Rev. B **81**, 024107 (2010).

[3] C. C. Liu, H. Jiang and Y. Yao, Phys. Rev. B **84**, 195430 (2011).

[4] C. C. Liu, W. Feng, and Y. Yao, Phys. Rev. Lett. **107**, 076802 (2011).

[5] N. D. Drummond, V. Zolyomi, and V. I. Falko, Phys. Rev. B 85, 075423 (2012).

[6] M. Ezawa, Phys. Rev. Lett. 109, 055502 (2012).

[7] D. Chiappe, C. Grazianetti, G. Tallarida, M. Fanciulli, and A. Molle, Adv. Mater. 24, 5088 (2012).

[8] A. Fleurence, R. Friedlein, T. Ozaki, H. Kawai, Y. Wang Y. Yamada-Takamura, Phys. Rev. Lett. **108**, 245501 (2012).

[9] L. Meng, Y. Wang, L. Zhang, S. Du, R. Wu, L. Li, Y. Zhang, G. Li, H. Zhou, et al. Nano Lett. **13**, 685 (2013).

[10] P. D. Padova, C. Quaresima, C. Ottaviani, P. M. Sheverdyaeva, P. Moras, C. Carbone, D.

Topwal, B. Olivieri, A. Kara, H. Oughaddou, B. Aufray and G. L. Lay, Appl. Phys. Lett. **96**,261905 (2010).

[11] B. Aufray, A. Kara, S. Vizzini, H. Oughaddou, C. Léandri, B. Ealet and G. Le Lay, Appl. Phys. Lett., **96**, 183102 (2010).

[12] T. T. Wu, X. F. Wang, M. X. Zhai, H. Liu, L. P. Zhou, and Y. J. Jiang, Appl. Phys. Lett. **100**, 052112 (2012).

[13] C. Jiang, X. F. Wang and M. X. Zhai, Carbon, **68**, 406, (2014).

[14] J. Munárriz, C. Gaul, A. V. Malyshev, P. A. Orellana, C. A. Müller, and F. Domínguez-Adame, Appl. Phys. Lett. **88**, 155423 (2013).

[15] J. Kang, F. Wu and J. B. Li, Appl. Phys. Lett. **100**, 233122 (2012).

[16] C. Y. Xu, G. F. Luo, Q. H. Liu, J. X. Zheng, Z. M. Zhang, S. G. Nagase, Z. X. Gao, and J. Lu, Nanoscale **4**,3111 (2012).

[17] A. B. Chen, X. F. Wang, P. Vasiopoulous, M. X. Zhai, and Y. S. Liu, Phys. Chem. Chem. Phys. **16**, 5113 (2014).

[18] L. Pan, H. J. Liu, X. J. Tan, H. Y. Lv, J. Shi, X. F. Tang and G. Zheng, Phys. Chem. Chem. Phys. **14**, 13588 (2012).

[19] K.Zberecki, M.Wierzbicki, J. Barnaś, R. Swirkowicz, Phys. Rev. B **88**, 115404 (2013)

[20] K. Zberecki ,R. Swirkowicz, J. Barnaś Phys. Chem. Chem. Phys. **16**, 12900 (2014).

[21] K. Uchida, S. Takahashi, K. Harii, J. Ieda, W. Koshibae, K. Ando, S. Maekawa, and E. Saitoh, Nature (London) 455, 778 (2008).

[22] H. Adachi, J. Ohe, S. Takahashi, and S. Maekawa, Phys. Rev. B **83**, 094410 (2011).

[23] C. M. Jaworski, R. C. Myers, E. Johnston-Halperin and J. P. Heremans, Nature, (London) **487**, 210 (2012).

[24] M. Weiler, M. Althammer, F. D. Czeschka, H. Huebl, M. S. Wagner, M. Opel, I. M. Imort, G.

Reiss, A. Thomas, R. Gross, and T. B. Goennenwein, Phys. Rev. Lett.108, 106602 (2012).

[25] K. Uchida, T. Nonaka, T. Kikkawa, Y. Kajiwara, and E. Saitoh, Phys. Rev. B, **87**, 104412 (2013).

[26] M. G. Zeng, W. Huang, and G. C. Liang, Nanoscale, **5**, 200 (2013).

[27] Y. S. Liu, X. F. Yang, F. Chi, M. S. Si, and Y. Guo, Appl. Phys. Lett. **101**, 213109 (2012).

[28] Y. S. Liu, X. F. Wang and F. Chi, J. Mater. Chem. C, **1**, 8046 (2013).

[29] X. F. Yang, Y. S. Liu, X. Zhang, L. P. Zhou, X. F. Wang, and J. F. Feng, Phys. Chem. Chem. Phys. **16**, 11349 (2014).

[30] Y. S. Liu, X. Zhang, X. F. Wang, and J. F. Feng, Appl. Phys. Lett. **16**, 11349 (2014).

[31] X. F. Yang, Y. S. Liu, X. F. Wang, and J. F. Feng, AIP advances **4**, 087116 (2014).

[32] Z. Y. Zhao, X. C. Zhai and G. J. Jin, Appl. Phys. Lett. **101**, 083117 (2012).

[33] J. Kang, F. Wu, S. S. Li, J. B. Xia, and J. B. Li, Appl. Phys. Lett. **100**, 153102 (2012).

[34] Y. Oeiras, F. M. Araújo-Moreira, and E. Z. da Silva, Phys. Rev. B **80**, 073405 (2009).

[35] X. H. Zheng, I. Rungger, Z. Zeng and S. Sanvito, Phys. Rev. B **80**, 235426 (2009).

[36] R. T. Lv, Q. Li, A. R. Botello-Mendez, T. Hayashi, B. Wang, A. Berkdemir et. al. Scientific reports. **2**, 586 (2012).

[37] S. Dutta, A. K. Manna, and S. K. Pati, Phys. Rev. Lett. **102**, 096601 (2009).

[38] K. Raidongia et. al. J. Mater. Chem. **18**, 83 (2008).

[39] K. Zberecki, R. Swirkowicz, and J. Barnaś, Phys. Rev. B **89**, 165419 (2014).

[40] A. Lopez-Bezanilla, J. Phys. Chem. C **118**, 18788 (2014).

[41] T. Taylor, H. Guo, and J. Wang, Phys. Rev. B **63**, 245407 (2001).

[42] M. Brandbyge, J. L. Mozos, P. Ordejon, J. Taylor, and K. Stokbro, Phys. Rev. B **65**, 165401 (2002).

[43] F. Muñoz-Rojas, J. Fernánde-Rossier, and J. J. Palacios, Phys. Rev. lett. **102**, 136810 (2009).

[44] J. H. Zhu, S. Y. Wei, N. Haldolaarachchige, J. He, D. P. Young and Z. H. Guo, Nanoscale, **4**, 152 (2012).

[45] H X. Luan, C. W. Zhang, F. B. Zheng and P. J. Wang, J. Phys. Chem. C, **117**, 13620 (2013).

[46] K. Kobayashi, H. Aikawa, S. Katsumoto and Y. Iye , Phys. Rev. Lett. **88** 256806 (2002).

[47] Y. Dubi and M. Di Ventra, Phys. Rev. B **79**, 081302(R) (2009).

[48] X. F. Yang and Y. S. Liu, J. Appl. Phys. **113**, 164310 (2013).

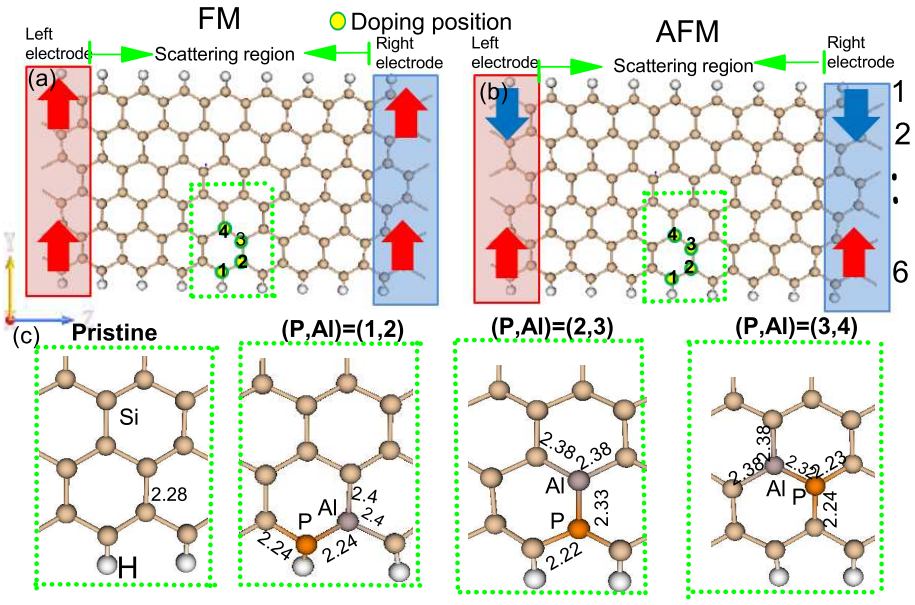

FIG. 1: Two-probe structures of 6-ZSiNR in the FM (a) and AFM (b) quantum states. Some bond lengths (in Å) near the doping positions are shown in (c). The label (n,m) denotes the a P atom doped at n position and meanwhile an Al atom doped at m position. n and m positions are indicated in Figs. 1(a) and (b).

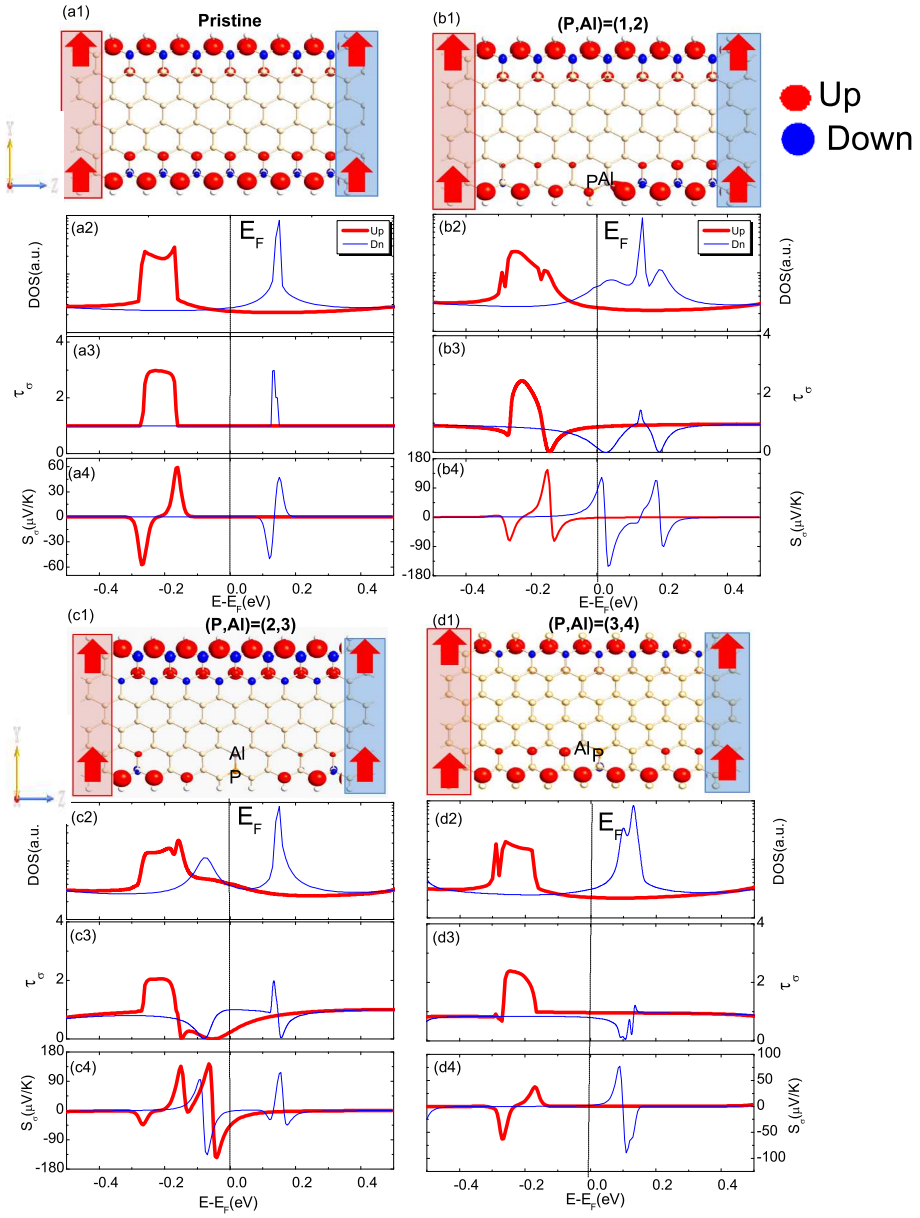

FIG. 2: (Color online) Spin density distributions of the 6-ZSiNRs on the central scattering region (a1,b1,c1,d1), and spin-dependent DOSs (a2,b2,c2,d2), spin-dependent transmission function τ_σ (a3,b3,c3,d3), and spin-dependent Seebeck coefficient S_σ (a4,b4,c4,d4) as functions of the electron energy for the pristine and Al-P doped FM ZSiNRs, respectively. The thick red lines represent the spin-up components and the thin blue lines mean the spin-down ones. The dotted lines denote the Fermi level. The direction and amplitude of the spin polarization on each atom are indicated by the color (up in red, down in blue) and the radius of the filled circle on the atom sphere, respectively. The electrode temperature T is 70 K.

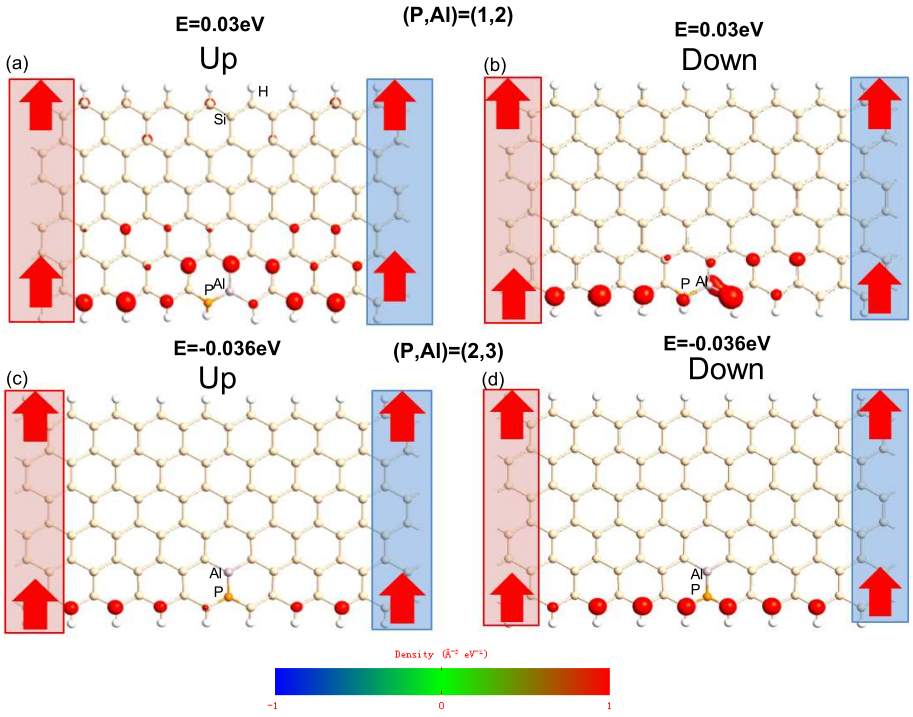

FIG. 3: (Color online) (a) Spin-up LDOS at $E = 0.03eV$ for the (1,2) doping. (b) Spin-down LDOS at $E = 0.03eV$ for the (1,2) doping. (c) Spin-up LDOS at $E = -0.036eV$ for the (2,3) doping. (d) Spin-down LDOS at $E = -0.036eV$ for the (2,3) doping.

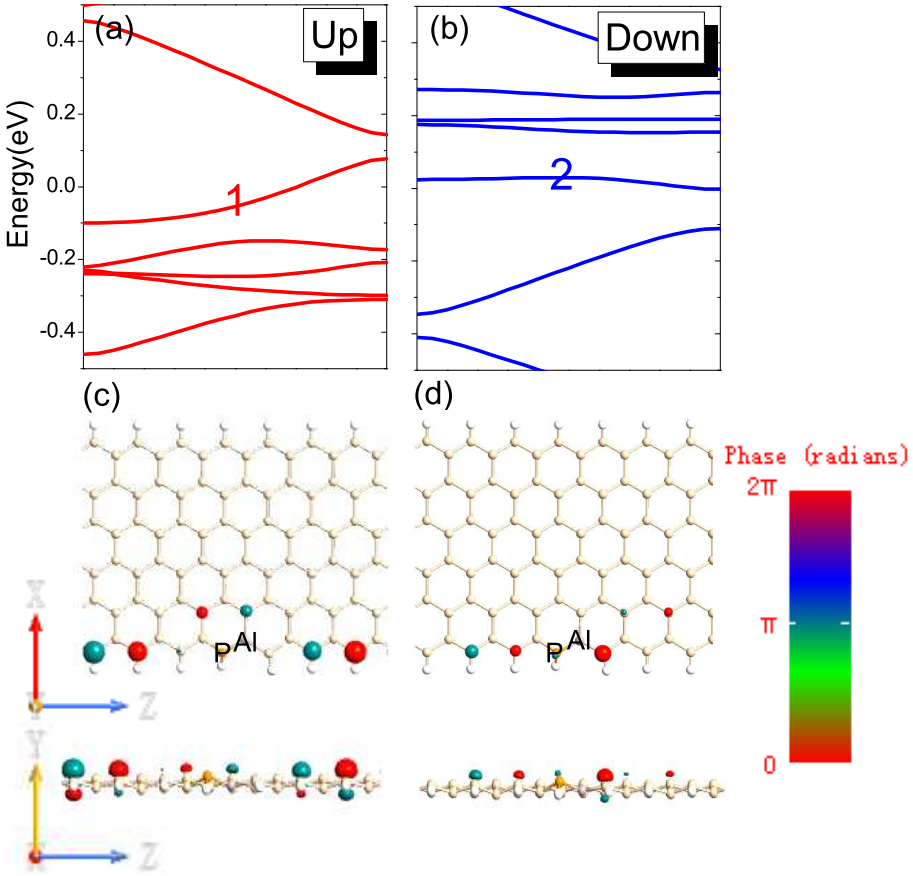

FIG. 4: (Color online) Spin-resolved energy band structures for the (1,2) doping in the FM ZSiNR, and the wave functions of the energy band 1 for spin-up component and 2 for the spin-down case. Different colors represent the different phases.

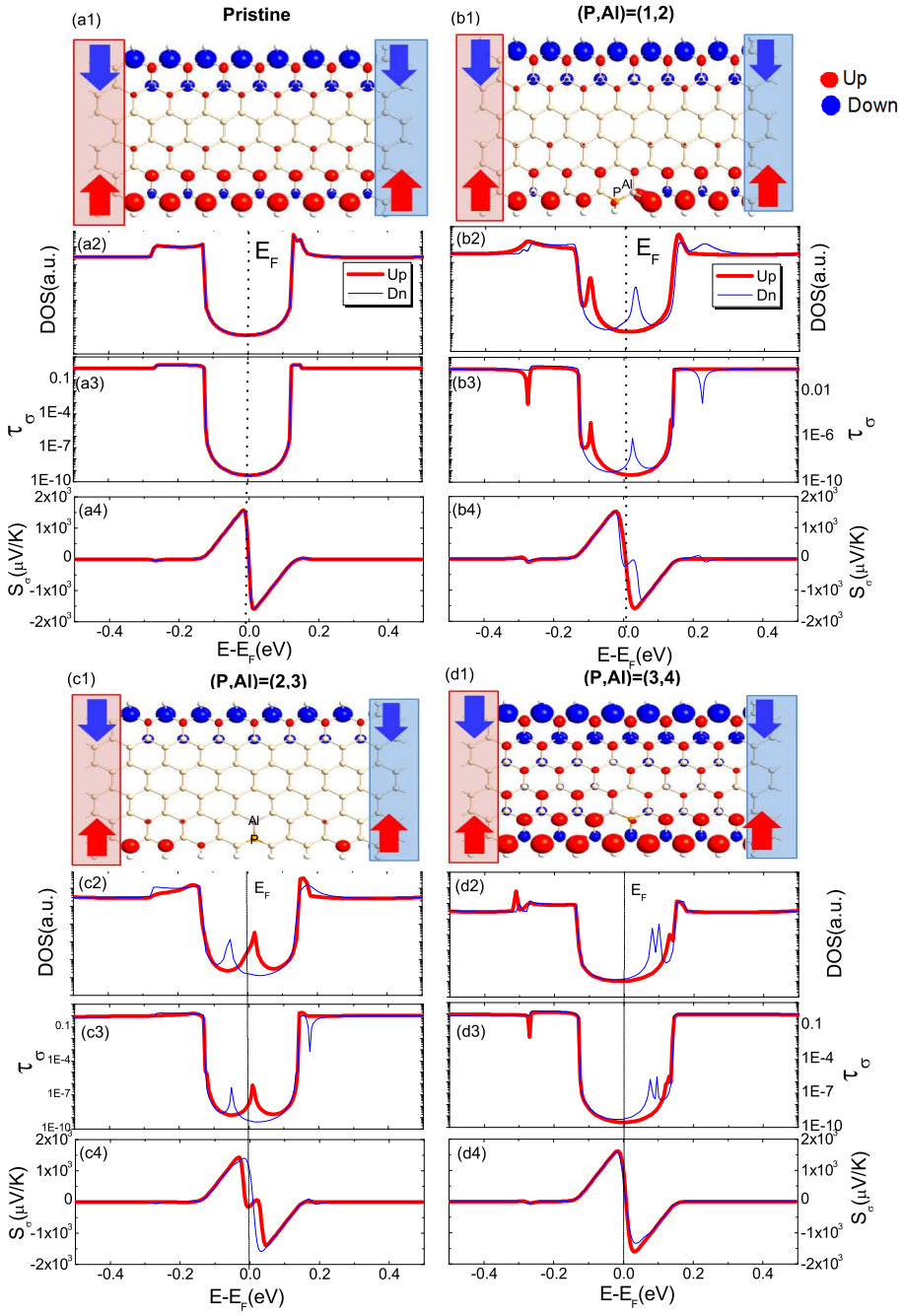

FIG. 5: (Color online) Spin density distributions of the 6-ZSiNRs on the central scattering region (a1,b1,c1,d1), log-plot of spin-dependent DOSs (a2,b2,c2,d2), log-plot of spin-dependent transmission function τ_σ (a3,b3,c3,d3), and spin-dependent Seebeck coefficient S_σ (a4,b4,c4,d4) as functions of the electron energy for pristine and Al-P doped AFM ZSiNRs. The thick red lines represent the spin-up components and the thin blue lines mean the spin-down ones. The dotted lines denote the Fermi level. The direction and amplitude of the spin polarization on each atom are indicated by the color (up in red, down in blue) and the radius of the filled circle on the atom sphere, respectively. The electrode temperature T is 70 K.

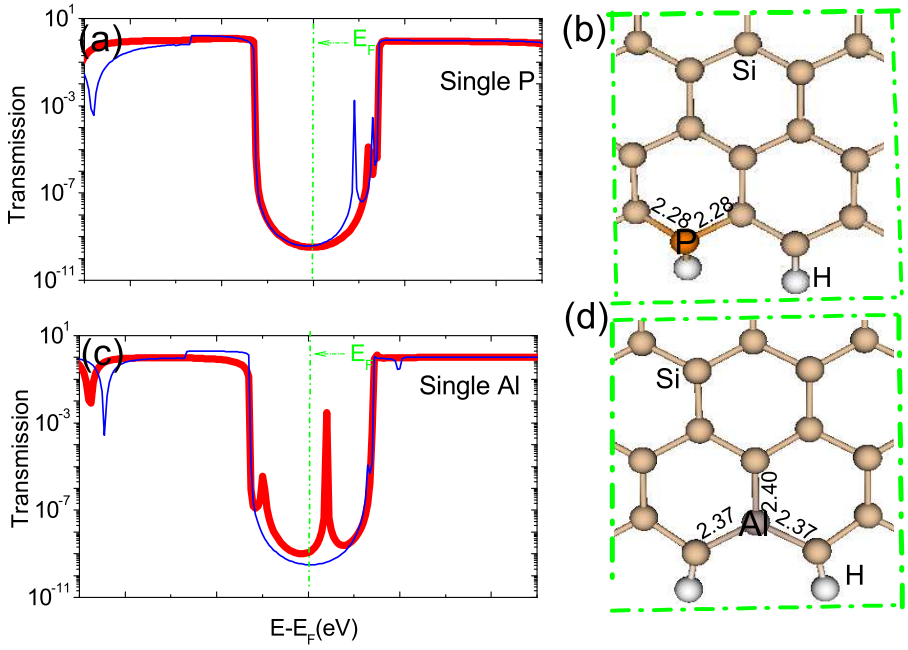

FIG. 6: (Color online) Log-plot of spin-dependent transmission function τ_σ as a function of the electron energy for (a) the single P atom doping and (b) the single Al atom doping. The thick red lines represent the spin-up components and the thin blue lines mean the spin-down ones. The dotted lines denote the Fermi level. The corresponding bond lengths (in Å) near the doping positions are shown in (b) and (d).

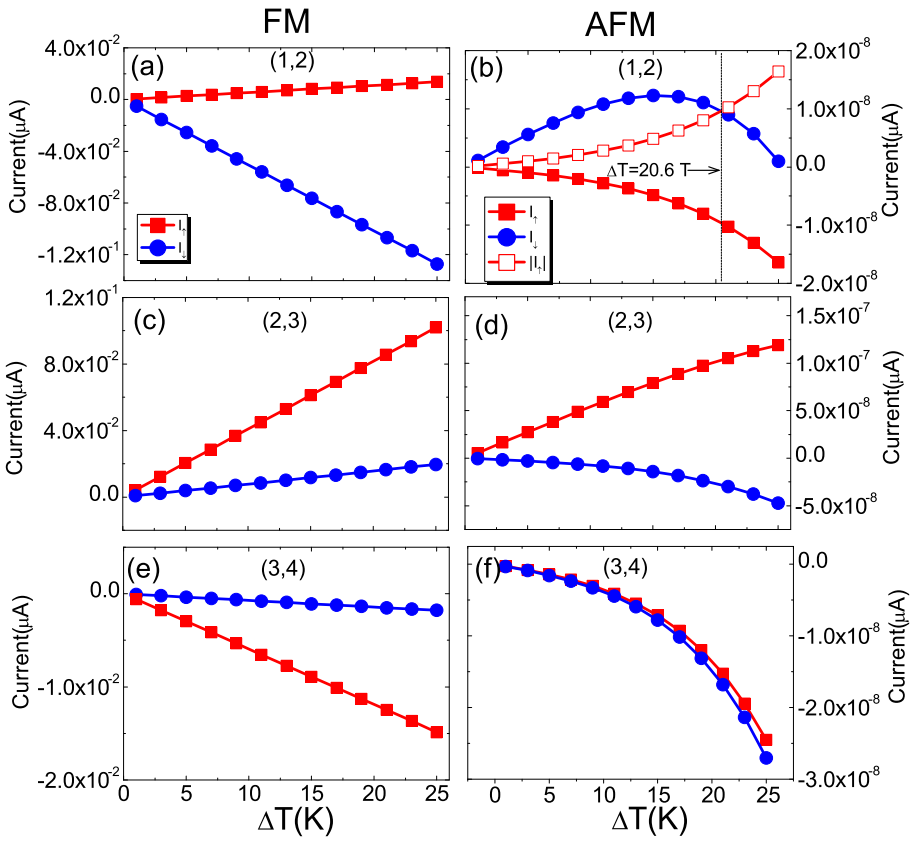

FIG. 7: (Color online) I_σ of the doped FM (the left column) and AFM (the right column) ZSiNRs as function of ΔT for $T = 70K$.

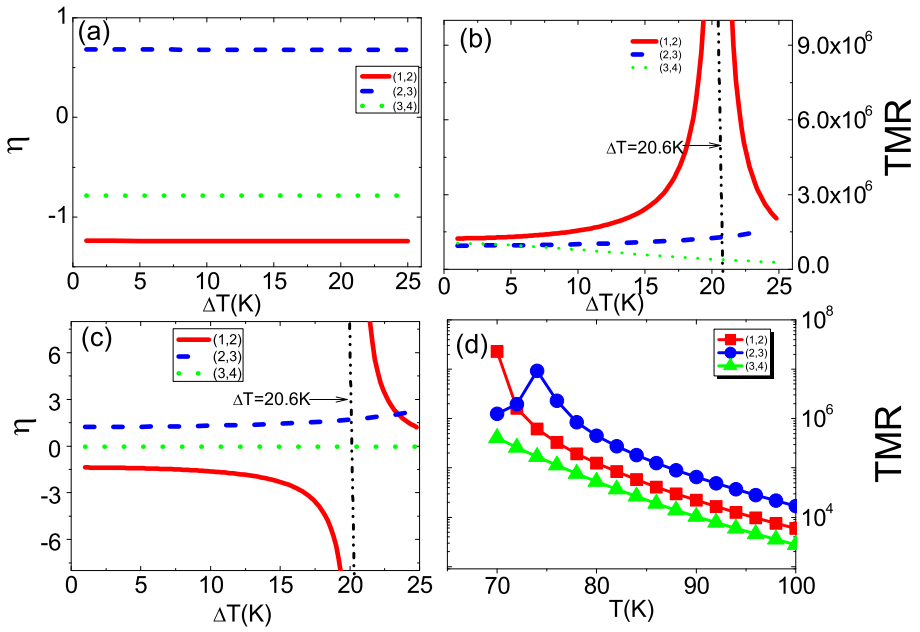

FIG. 8: (Color online) SFE of the three doped (a) FM and (c) AFM ZSiNRs as functions of ΔT for $T = 70K$. (b) TMR of the three doped ZSiNRs as a function of ΔT for $T = 70K$. (d) Log-plot of the TMR of the three doped ZSiNRs as functions of T for $\Delta T = 20K$.